NASA Technical Memorandum 79081

MODAL PROPAGATION ANGLES IN DUCTS WITH SOFT WALLS AND THEIR CONNECTION WITH SUPPRESSOR PERFORMANCE

Edward J. Rice
Lewis Research Center
Cleveland, Ohio

TECHNICAL PAPER to be presented at the
Fifth Aeroacoustics Conference
sponsored by the American Institute of Aeronautics and Astronautics
Seattle, Washington, March 12-14, 1979

MODAL PROPAGATION ANGLES IN DUCTS WITH SOFT WALLS AND THEIR CONNECTION WITH SUPPRESSOR PERFORMANCE

Edward J. Rice*
National Aeronautics and Space Administration
Lewis Research Center
Cleveland, Ohio

E-9662

Abstract

The angles of propagation of the wave fronts associated with duct modes are derived for a cylindrical duct with soft walls (acoustic suppressors) and a uniform steady flow. The angle of propagation with respect to the radial coordinate (angle of incidence on the wall) is shown to be a better correlating parameter for the optimum wall impedance of spinning modes than the previously used mode cutoff ratio. Both the angle of incidence upon the duct wall and the propagation angle with respect to the duct axis are required to describe the attenuation of a propagating mode. Using the modal propagation angles, a geometric acoustics approach to suppressor acoustic performance was developed. Results from this approximate method were compared to exact modal propagation calculations to check the accuracy of the approximate method. The results are favorable except in the immediate vicinity of the modal optimum impedance where the approximate method yields about one-half of the exact maximum attenuation.

Introduction

The angles of propagation for the wave fronts making up an acoustic mode are derived for ducts with soft walls (acoustic liner). These are the angles which the velocity vector normal to the local wave front makes with the three coordinate axes. The angles associated with the group velocity vector are also derived. This effort is an extension of the work of Ref. 1 in which both approximate and exact wave propagation angles were derived for a cylindrical duct with uniform steady flow. In Ref. 1, only the hardwall results were given and the emphasis was on the relationship of the propagation angles in the duct and the far-field radiation pattern. This paper will consider ducts with soft walls and the relationship of the propagation angles to acoustic liner performance.

In Refs. 2 to 4 the optimum acoustic impedance and the maximum possible attenuation for an acoustic mode were shown to be intimately connected to and correlated by the mode cut-off ratio. The mode cut-off ratio is a somewhat abstract parameter, particularly for soft wall ducts, and an explanation of its effectiveness as a correlation parameter was that it was connected to the angle of incidence upon the liner wall. This paper formalizes this connection and shows that angle of incidence is the more fundamental parameter and in fact correlates the optimum impedance values better than does the cut-off ratio.

The maximum possible attenuation for a mode was also shown to be approximately correlated by the cut-off ratio. However, the collapse of these attenuation curves was not as good as desired and some large errors could occur particularly near mode cut-off when using this correlation. A simple geometric approach similar to that of Ref. 5 was tried. This approach considers that the number of encounters that the wave has with the soft wall is determined by the wave angle with respect to the duct axis and by the duct size. The acoustic power remaining after each encounter with the wall is related to angle of incidence and the wall impedance properties. When these two concepts are combined in a simple model, the acoustic power attenuation for the mode can be calculated. The resulting equation is shown to be exact for a rectangular duct without Mach number and for only slightly soft walls. This approximate method is extended to include cylindrical ducts and uniform duct flow. Results from the approximate model are compared with the exact attenuation results for several conditions including acoustic impedances up to the optimum for both rectangular and cylindrical ducts with flow.

The purpose of this paper is to provide the foundation for a simple geometric acoustics approach which may be useful for complex suppressor geometries and multimodal noise sources for which exact methods are inefficient and extremely difficult.

Symbols

c	speed of sound, or the magnitude of the wave velocity vector normal to a plane wave front, m/sec
c_i	components of vector c, $i = x, r, \Phi$, m/sec
c_R	resultant velocity vector, $\sqrt{c_x^2 + c_r^2}$, m/sec
D	duct diameter, m
f	frequency, Hz
H	rectangular duct height, m
I_F	axial acoustic intensity leaving end of suppressor, N/m sec
I_I	axial acoustic intensity entering suppressor, N/m sec
I_x^-	axial acoustic intensity of reflected wave off soft wall, N/m sec
I_x^+	axial acoustic intensity of incidence wave on soft wall, N/m sec
i	$\sqrt{-1}$
J_m	Bessel function of the first kind of order m
j	rectangular duct mode number
k	wave number, ω/c, m^{-1}
k_r	radial wave number, m^{-1}
$k_{r\Phi}$	combined radial-circumferential wave number (α/r_o), m^{-1}
k_x	axial wave number, m^{-1}
k_Φ	circumferential wave number, m^{-1}
L	suppressor length, m
M	Mach number of uniform steady duct flow
M_o	Mach number of uniform outside of boundary layer
m	spinning mode lobe number
P	acoustic pressure, N/m^2
r	radial coordinate, m
r_o	duct radius, m

*Head-Acoustics Section, Member AIAA

R	magnitude of complex eigenvalue
t	time, sec
x	axial coordinate, m
Δx	axial distance between encounters of acoustic wave with duct walls, m
y	transverse rectangular coordinate normal to duct walls, m
z	transverse rectangular coordinate parallel to duct walls, m
α	complex eigenvalue, $Re^{i\varphi}$
β	real part of complex quantity, see Eqs. (12), (13)
δ	boundary layer thickness for 1/7th power velocity profile, m
ϵ	dimensionless boundary layer thickness, δ/r_o
η	frequency parameter, fD/c or fH/C
θ	specific acoustic resistance
θ_m	optimum specific acoustic resistance
μ	radial mode number
ξ	mode cut-off ratio, see Eq. (22)
σ	attenuation or damping coefficient, see Eq. (7)
τ	propagation coefficients, see Eqs. (7), (8)
Φ	circumferential coordinate, radians
φ	phase of eigenvalue α, radians
φ_r	wave front propagation angle relative to radial coordinate, angle of incidence on the wall, deg
φ_x	wave front propagation angle relative to axial coordinate, deg
φ_y	wave front propagation angle measured from y coordinate, deg
φ_Φ	wave front propagation angle relative to circumferential coordinate, deg
X	specific acoustic reactance
X_m	optimum specific acoustic reactance
Ψ_x	resultant axial propagation angle in duct, deg
Ψ_r	resultant propagation angle measured from radial coordinate, deg
Ψ_Φ	resultant propagation angle measured from circumferential coordinate, deg
ω	circular frequency, radians/sec

Subscripts:

i	equal to x, r, or Φ
$m\mu$	mode indices, m lobe μ radial order
R	indicates real part of complex quantity
r_o	evaluated at outerwall

Development of the Propagation Angles

The initial development of the expressions for the propagation angles can proceed exactly as in Ref. 1. The wave equation in a circular duct with a steady flow can be expressed as

$$(1 - M^2)\frac{\partial^2 P}{\partial x^2} - \frac{2M}{c}\frac{\partial^2 P}{\partial x \partial t} + \frac{\partial^2 P}{\partial r^2} + \frac{1}{r}\frac{\partial P}{\partial r} + \frac{1}{r^2}\frac{\partial^2 P}{\partial \Phi^2} = \frac{1}{c^2}\frac{\partial^2 P}{\partial t^2} \qquad (1)$$

where x, r, and Φ are the usual cylindrical coordinates, t is time, M is Mach number, c the speed of sound, and P is the acoustic pressure. The solution to Eq. (1) for the pressure is,

$$P_{m\mu} = J_m\left(\frac{\alpha_{m\mu} r}{r_o}\right) e^{i\omega t - ik_{x,m\mu}x - im\Phi} \qquad (2)$$

where m is the number of lobes for the spinning mode (the transverse order), μ is the radial order number of the mode, $k_{x,m\mu}$ is the axial wave number, ω is the circular frequency, r_o is the outer wall radius, $\alpha_{m\mu}$ is the eigenvalue of the $m\mu$ mode, and J_m is the Bessel function of the first kind and order m.

Wave Numbers and the Phase Velocity Propagation Angles

For brevity, the $m\mu$ subscripts will be deleted from here on, and it will be understood that a single (but quite general) mode is being considered. When Eq. (2) is inserted into Eq. (1) the result is,

$$\left(\frac{\alpha}{r_o}\right)^2 + k_x^2 = k^2 - 2Mkk_x + M^2k^2 = (k - Mk_x)^2 \qquad (3)$$

The first term in Eq. (3) is a combined radial-transverse wave number squared which could be denoted by,

$$\frac{\alpha}{r_o} = k_{r\Phi} \qquad (4)$$

This combination of wave numbers is the cause of the trouble in defining some of the propagation angles in cylindrical ducts.

The i^{th} propagation angle can be shown (for hardwall ducts),[1] to be given by,

$$\cos\varphi_i = \frac{k_i}{\sqrt{\sum_i k_i^2}} = \frac{k_i}{k\left(1 - M\frac{k_x}{k}\right)} \qquad (5)$$

where $i = r, \Phi$, or x, and φ_i is the angle between the normal to the wave front and the i^{th} coordinate axis, and the denominator of Eq. (5) was obtained from Eq. (3). The angles φ_x, φ_r and φ_Φ can be seen in Fig. 1. The vector c is normal to the local wavefront. The other angle set Ψ_i and the resultant vector c_R due to additional convective effects also shown in Fig. 1 will be discussed later.

Before proceding further, one must recognize that, due to the soft wall boundary condition, the quantities α and k_x in Eq. (3) are complex numbers Only the real parts of the wave number are related to propagation wave numbers for use in Eq. (5) while the imaginary parts represent damping terms. The axial wave number can be rewritten as,

$$k_x = k(\tau - i\sigma) \qquad (6)$$

and this along with Eq. (3) yields,

$$\sigma + i\tau = \frac{-iM + i\sqrt{1 - (1 - M^2)\left(\frac{\alpha}{\pi\eta}\right)^2}}{1 - M^2} \qquad (7)$$

and thus,

$$\tau = \frac{-M + \frac{1}{\sqrt{2}}\left[1 - (1 - M^2)\left(\frac{R}{\pi\eta}\right)^2 \cos 2\varphi + \sqrt{1 + (1 - M^2)\left(\frac{R}{\pi\eta}\right)^4 - 2(1 - M^2)\left(\frac{R}{\pi\eta}\right)^2 \cos 2\varphi}\right]^{1/2}}{1 - M^2} \tag{8}$$

where R and φ are the amplitude and phase of the complex eigenvalue α and the frequency parameter is,

$$\eta = \frac{\omega r_o}{\pi c} = \frac{fD}{c} \tag{9}$$

Equation (8) is obtained by solving for the imaginary part of Eq. (7).

To obtain the angle of incidence at the liner wall (φ_r) in a simple form, the assumption is made that the combined radial-transverse complex wave number can be split as follows,

$$k_{r\Phi}^2 = \left(\frac{\alpha}{r_o}\right)^2 = k_r^2 + k_\Phi^2 = k_r^2 + \left(\frac{m}{r}\right)^2 \tag{10}$$

This assumption was used in Ref. 1 for hardwall ducts and was found to provide adequate results near the outer wall when compared to an exact solution using Hankel functions. The real part of $k_r(k_{r,R})$ for use in Eq. (5) can then be obtained as,

$$k_{r,R} = \text{Real}\sqrt{\left(\frac{\alpha}{r_o}\right)^2 - \left(\frac{m}{r}\right)^2} = \frac{k}{\pi\eta}\,\text{Real}\sqrt{\alpha^2 - \left(\frac{mr_o}{r}\right)^2} \tag{11}$$

The propagation angles will be calculated only at the outer wall ($r = r_o$) where the approximations used here are reasonably accurate.[1] Let,

$$k_{r,R}\Big)_{r_o} = \frac{k\beta}{\pi\eta} \tag{12}$$

thus

$$\beta = \frac{1}{\sqrt{2}}\left(R^2 \cos 2\varphi - m^2 + \sqrt{R^4 - 2m^2R^2 \cos 2\varphi + m^4}\right)^{1/2} \tag{13}$$

The circumferential wave number (at the outer wall) as seen from Eq. (10) is,

$$k_\Phi = \frac{m}{r_o} = \frac{mk}{\pi\eta} \tag{14}$$

which is real unlike the k_x and k_r.
The real parts of the wave numbers can now be used in Eq. (5) to obtain,

$$\cos\varphi_x = \frac{\tau}{\sqrt{\tau^2 + \left(\frac{\beta}{\pi\eta}\right)^2 + \left(\frac{m}{\pi\eta}\right)^2}} \tag{15}$$

$$\cos\varphi_r = \frac{\beta}{\pi\eta\sqrt{\tau^2 + \left(\frac{\beta}{\pi\eta}\right)^2 + \left(\frac{m}{\pi\eta}\right)^2}} \tag{16}$$

$$\cos\varphi_\Phi = \frac{m}{\pi\eta\sqrt{\tau^2 + \left(\frac{\beta}{\pi\eta}\right)^2 + \left(\frac{m}{\pi\eta}\right)^2}} \tag{17}$$

Group Velocity Propagation Angles

Equations (15) to (17) describe the orientation of the wave front at the outer wall of the circular duct and can be seen to include the duct Mach number through the propagation coefficient τ. There is an additional Mach number effect as shown in Fig. 1 which causes a drift in the axial velocity and produces a resultant vector (c_R) of propagation which is not normal to the wavefront. This vector is associated with the group velocity[1] and the angles of propagation associated with c_R will be of use in a later discussion. These angles can be derived from the geometry shown in Fig. 1 using the fact that the vector cM alters only the x component of velocity but not c_r or c_Φ. These angles can be expressed as,

$$\cos\psi_x = \frac{M + \cos\varphi_x}{\sqrt{1 + M^2 + 2M\cos\varphi_x}} \tag{18}$$

$$\cos\psi_r = \frac{\cos\varphi_r}{\sqrt{1 + M^2 + 2M\cos\varphi_x}} \tag{19}$$

and

$$\cos\psi_\Phi = \frac{\cos\varphi_\Phi}{\sqrt{1 + M^2 + 2M\cos\varphi_x}} \tag{20}$$

Correlation of Optimum Impedance with Incidence Angle

The angle of incidence on the soft wall (Eq. (16)) was used to correlate some of the optimum impedance calculations reported in Ref. 4. These calculations were made for a cylindrical duct with a 1/7th power boundary layer and a uniform core flow outside of the boundary layer. Standard modal solutions were used within the core flow and were coupled to the wall impedance by a Runge-Kutta integration through the boundary layer. These correlations are shown in Figs. 2 and 3. These calculations include several lobe numbers (m) and the entire range of radial modes from well propagating to near cut-off. Comparison of Figs. 2 and 3 with Figs. 12 and 13 of Ref. 4 show that the angle of incidence correlates the modal optimum impedance somewhat better than the mode cut-off ratio did in Ref. 4. Using cut-off ratio[4] the first radial mode for $m = 5$ showed some deviation from the correlation while $m = 9$ and 16 had quite pronounced deviations. This deviation does not appear when incidence angle is used. This improvement can be most easily explained by using the hardwall incidence angle given in Ref. 1 which was

$$\cos\varphi_r\Big]_{r_o} = \frac{\sqrt{1 - M^2}\sqrt{1 - \left(\frac{m}{\alpha}\right)^2}}{\xi\left(1 - M\sqrt{1 - 1/\xi^2}\right)} \tag{21}$$

where the cut-off ratio ξ is given by

$$\xi = \frac{kr_o}{\alpha\sqrt{1 - M^2}} \qquad (22)$$

For higher radial modes ($\alpha \gg m$) or for small m the term $\sqrt{1 - (m/\alpha)^2}$ approaches unity. Equation (21) then shows that for constant Mach number M (as used in Figs. 2 and 3) the angle of incidence (φ_r) is a function only of cut-off ratio and either parameter is sufficient to correlate the optimum impedance. However, for large m and low radial order $\alpha \approx m$, the term $\sqrt{1 - (m/\alpha)^2}$ in Eq. (21) influences the incidence angle and causes scatter in the correlation as shown in Ref. 4. At sufficiently high lobe numbers the splitting of the radial and transverse wave numbers as used in Eq. (10), a rectangular coordinate approximation to the cylindrical coordinate system, will lose validity and some scatter in the correlation will again be introduced. This latter problem can probably be overcome by extending the exact Hankel function solutions of Ref. 1 to soft walls.

The optimum impedance correlation shown in Figs. 2 and 3 were for propagation calculations containing a boundary layer. The angle of incidence calculated in each case was valid only in the uniform flow region outside the boundary layer. A complete geometric approach to duct propagation must contain the refractive effects on the acoustic wave as it passes through this boundary layer. This is emphasized by the calculated optimum impedances shown in Figs. 4 and 5 for three boundary layer thicknesses. Note that for angles of incidence (φ_r) above 65° there is a dramatic effect of boundary layer thickness upon optimum resistance (Fig. 4) while the reactance (Fig. 5) is affected down to about 50°. For a given set of propagation angles outside of the boundary layer there is a unique optimum impedance but the boundary layer acts as an impedance transformer between the uniform flow region and the wall. Fortunately for modes nearer to cut-off, the wave motion is not directed into the velocity gradients (mainly radial or circumferential) and the boundary layer has much less effect upon the propagation of these modes.

An alternate correlation of one set of calculations ($\epsilon = 0.005$) in Fig. 5 is shown in Fig. 6. Here the resultant incidence angle (ψ_r) is used rather than φ_r. Recall that ψ_r contains the axial velocity drift effect and is associated with the group velocity. Some of the scatter in the points nearer cut-off (small incidence angle) may have been reduced by using ψ_r and the numerical value of incidence angle indicates more of a normal incidence than does φ_r ($\psi_r < \varphi_r$). The ψ_i seem to have more physical significance than the φ_i. For example in Ref. 1 it was shown that $\psi_x \to 90°$ at mode cut-off while φ_x does not.

From the above discussion it is thus proposed that the angle of incidence of the wave fronts on the lined wall is a more fundamental and obviously more easily visualized parameter than the mode cut-off ratio for correlating liner optimum impedance. However, the mode cut-off ratio is still considered to be an extremely useful parameter for liner design purposes with the previous discussion serving to explain the reason for its effectiveness and pointing out its limitations.

Estimation of Attenuation Using Propagation Angles

The previous section dealt only with the connection of optimum impedance with wave angle of incidence. To complete the discussion some estimate of sound power attenuation must be made. An estimate of liner performance can be obtained using the method of Ref. 3 along with the improved impedance correlations of Ref. 4. Both of these references are based upon mode cut-off ratio. However, in this section a geometric approach similar to those of Refs. 5 and 6 will be used. This ray acoustics approach using the propagation angles derived in the previous section clearly illustrates the important aspects of the sound propagation phenomena in lined ducts which are usually obscured in the physical acoustics approach. It is all the more satisfactory if usable results for liner design can be obtained. The first example will consider the simple two dimensional rectangular system without flow to illustrate the principles and provide motivation for an expectation of useful results. The analysis will then be extended to include uniform flow in a rectangular duct. Using these principles an acoustically lined cylindrical duct will then be considered.

Rectangular Two Dimensional Duct, M = 0

Figure 7 shows a rectangular duct without flow with a transverse mode propagating and bouncing between the soft walls. The angle of incidence between the velocity vector normal to these waves and the y coordinate is φ_y while the angle of the waves with respect to the duct axis is φ_x. The axial distance between encounters between the wave and the soft wall is,

$$\Delta x = \frac{H}{\tan \varphi_x} \qquad (23)$$

where H is the duct height. The total number of wall bounces in a duct of length L is then

$$N = \frac{L}{\Delta x} = \frac{L}{H} \tan \varphi_x \qquad (24)$$

The ratio of axial flux after a wall bounce compared to the incident wave is given by

$$\frac{I_x^-}{I_x^+} = \frac{(\theta^2 + X^2)\cos^2\varphi_y - 2\theta \cos \varphi_y + 1}{(\theta^2 + X^2)\cos^2\varphi_y + 2\theta \cos \varphi_y + 1} \qquad (25)$$

where θ and X are the wall specific acoustic resistance and reactance. Note that Eq. (25) involves only the wall properties and the angle of incidence. Equation (25) was derived in the same way as the absorption coefficient is conventionally derived. A plane wave is assumed to be incident upon a plane absorber and the angle of reflection is equal to the angle of incidence. The absorption coefficient is $1 - I_x^-/I_x^+$.

After the N bounces in the duct the ratio of the final to initial axial acoustic intensity is,

$$\frac{I_F}{I_I} = \left(\frac{I_x^-}{I_x^+}\right)^N \qquad (26)$$

Since only one mode is considered here the attenuation can be obtained from the intensity ratio as,

$$\Delta dB = 10 \text{ Log } \frac{I_F}{I_I} = 10N \text{ Log } \frac{I_x^-}{I_x^+} \qquad (27)$$

Now consider the often studied problem of nearly hard walls which is quite a good approximation to the exact physical acoustics solutions except in the vicinity of the optimum impedance. With only slightly soft walls,

$$\frac{I_x^-}{I_x^+} \approx 1 - \frac{4\theta}{\cos \varphi_y(\theta^2 + \chi^2)} \qquad (28)$$

and

$$\text{Log } \frac{I_x^-}{I_x^+} \approx \frac{-4\theta}{\ln 10 \cos \varphi_y(\theta^2 + \chi^2)} \qquad (29)$$

Equations (28) and (29) were derived using Eq. (25) with the assumption that impedance is very large. To the first order of approximation, the axial propagation angle and the incidence angle for the j^{th} transverse mode are given by

$$\tan \varphi_x \approx \frac{j}{\eta \sqrt{1 - (j/\eta)^2}} \qquad (30)$$

and

$$\cos \varphi_y \approx \frac{j}{\eta} \qquad (31)$$

Equations (15) and (16) were used with y replacing r, m = 0, and the nearly hardwall approximation was used to evaluate the eigenvalues. When Eqs. (24), (29), (30), and (31) are used in Eq. (27) the result is,

$$\Delta dB \approx \frac{-17.37\ \theta\ (L/H)}{\sqrt{1 - (j/\eta)^2}\ (\theta^2 + \chi^2)} \qquad (32)$$

This equation for attenuation is exactly the same as would be obtained from the physical acoustics approach to the same nearly hardwall problem. Thus at least for rectangular ducts without steady flow and with wall impedance not in the vicinity of the optimum impedance, the ray acoustics approach using the angles of propagation and the acoustic flux loss per wall bounce gives very precise attenuations.

Rectangular Duct with Uniform Flow

With a finite Mach number in the duct Eq. (27) remains valid but the number of encounters of the wave with the wall (Eq. (24)) and the ratio of the incident to reflected axial intensity (Eq. (25)) must be modified. The number of bounces must now include the axial propagation angle associated with the group velocity (ψ_x). Equation (24) thus becomes,

$$N = \frac{L}{H} \tan \psi_x \qquad (33)$$

where Eq. (18) is used for ψ_x.

The ratios of axial intensities were derived as in the previous section with the addition that uniform flow must be considered in the wave equation and the continuity of displacement must be used at the soft wall. The derivation proceeds exactly as in Ref. 7, except that the relation between the wave numbers and the propagation angle was incorrectly expressed in Ref. 7 (effect of M on angles ignored). The axial intensity ratio (reflected to incident) is,

$$\frac{I_x^-}{I_x^+} = \Big[(\theta^2 + \chi^2)\cos^2\varphi_y(1 + M \sin \varphi_y)^2 - 2\theta \cos \varphi_y(1 + M \sin \varphi_y) + 1\Big] \Big/ \Big[(\theta^2 + \chi^2)\cos^2\varphi_y(1 + M \sin \varphi_y)^2 + 2\theta \cos \varphi_y(1 + M \sin \varphi_y) + 1\Big] \qquad (34)$$

Note that Eq. (34) reduces to Eq. (25) when M = 0.

For the approximate calculations to be shown later, Eqs. (15) and (16) were used with y replacing r and with m = 0. If a three dimensional rectangular duct calculation is desired with a transversly spinning wave considered, m could be retained and the z coordinate would just replace the Φ coordinate.

Cylindrical Duct with Uniform Flow

For a cylindrical duct with uniform steady flow the results of the previous section can be used directly as a first approximation. Of course φ_r must be used instead of φ_y in Eq. (34). As shown in Ref. 1, the approximations leading to Eqs. (15) to (17) are valid only near the outer wall because of curvature effects in the cylindrical duct. Equation (34) represents the physics of reflection and absorption which occur at the wall and it should thus remain valid. However, the number of encounters of the wave with the wall as expressed by Eq. (33) involves the propagation process throughout the entire depth or radius of the duct. For a rectangular duct ψ_x does not change with distance from the wall and Eq. (33) is thus valid. For a cylindrical duct, as discussed in Ref. 1, ψ_x is a function of radius and is always equal to 90° at the duct centerline. Thus using the value of ψ_x at the wall, as done here, will underestimate the number of bounces somewhat, and the approximate calculation of attenuation will be less than the exact attenuation. Some integrated value of ψ_x must be used rather than the value at the wall, but this has not yet been accomplished.

Comparison of Approximate and Exact Attenuations

A series of exact single mode propagation calculations were performed as in Ref. 8. These calculations were made for both rectangular and circular ducts. In each case a constant damping coefficient (σ) was used and the propagation coefficient (τ) was varied to produce a closed loop in the wall impedance plane (see Fig. 4, Ref. 8). Several points were used along this constant atten-

uation contour and the values of the variables needed to calculate the approximate attenuation (θ, χ, ζ, τ, R, φ) were recorded. Thus at these points the exact and approximate attenuations could be compared. The damping value was then increased, repeating the same procedure, until the damping contour collapsed to a point representing the maximum possible attenuation for the mode used. The results are presented in the following sections.

Rectangular Duct

The ratio of the attenuation by the approximate calculation using the geometrical acoustics approach to that of the exact physical acoustics calculations are shown in Fig. 8 for zero steady flow. The abscissa represents the degree of attenuation used for the calculations with the value of unity representing the maximum possible attenuation for this mode, the second symmetric mode. The symbols represent the average attenuation for the several points on a given exact damping contour while the bars represent the spread of these calculations. The averages are not unique, particularly where a large spread is present, since they depend upon the particular choice of points along the damping contour. Several observations can be made from Fig. 8. As damping is reduced (far from the optimum impedance) the approximate and exact attenuations are seen to be in better agreement with very little scatter. This agrees with the comments made pertaining to the limiting Eq. (32) which states that the approximate equation is exact far from the optimum impedance. Up to about one-half of the maximum attenuation the average attenuation around a contour is very good although considerable scatter occurs. As the optimum impedance is approached the approximate calculation gives only about one-half the attenuation as the exact calculation. At first glance, the 50 percent error possible here both at intermediate and high damping may appear unacceptable. However, the upper half of the damping range represents a very small portion of the impedance plane which would be very hard to realize precisely in a real application. Furthermore, in a multimodal excitation situation, where approximate techniques would be most valuable, a given wall impedance would be near to only a small fraction of the modal optima and errors involving only a few modes (assuming near equipartion of energy) would not seriously affect the final result. Also the apparently correct averaging where considerable scatter occurs would help the final multimodal result. The reason for the scatter observed will become more clear in a later discussion.

In Fig. 9 results are shown for the same mode as in Fig. 8 except that there is a steady inlet flow of $M = -0.4$. The results are much the same as in Fig. 8 with the low damping points showing agreement between approximate and exact attenuations which indicates that the Mach number effects were handled properly. Several points are shown at the intermediate damping point where the large scatter occurs. Two points are seen to be about 50 percent high while the bulk of the points on this damping contour are within about 20 percent of the exact attenuation.

To study the scattering of the approximate attenuation calculations, a complete scan over all values of propagation coefficient τ was made along a constant damping coefficient contour of $\sigma = 0.02$. The approximate to exact attenuation ratio is shown in Fig. 10 along with the incidence angle φ_y and the magnitude of the eigenvalue R. This scan involves several closed loops in the impedance plane and of course encompasses several modes. In Fig. 10(a) the scatter in approximate attenuation is seen to be a smooth oscillatory function. The scatter is seen to be small for the higher modes (mode number noted near top) and increases for the lower modes. The value of damping used for this calculation could not be attained by the first mode. There is no error at the borders of each mode and the average within a mode can be seen to be about unity in the attenuation ratio. If a cross plot were shown between Figs. 10(a) and (c) it would be seen that the scatter is cyclic with eigenvalue amplitude. The scatter seems to be least for the higher, near cut-off modes nearer to normal incidence (small φ_y) and to increase with angle of incidence. The generality of these results have not been tested.

Cylindrical Duct

Figure 11 shows comparisons of approximate and exact attenuations for a cylindrical duct for the second radial of a seven lobed spinning mode. The scatter is seen to be extremely small when compared to Figs. 8 and 9. This is probably due to the high frequency ($\eta = 20$ versus 5) as compared to the rectangular duct results. The same roll-off at high damping is seen here as in the rectangular duct. A difference occurs at low damping with the asymptote being about 0.9 rather than unity as previously seen. This is no doubt due to the underestimation of the number of encounters of the wave with the wall due to using the axial propagation at the wall rather than an integrated value over the duct. Recall that axial propagation angle is constant over a rectangular duct but increases to 90° at the center of a cylindrical duct.[1]

Concluding Remarks

The angle of incidence has been shown to be a more fundamental and more illuminating parameter than the mode cut-off ratio for correlating modal optimum impedances. The liner performance has been shown to involve both the angle of incidence and the axial angle of propagation along with the usual parameters of wall impedance and duct geometry. The use of these propagation angles in a ray acoustics propagation approach shows great promise although some additional effort is still needed to perfect this approach. If the ray acoustics approach can be perfected it would be an extremely powerful tool to solve problems in soft wall duct configurations which can not be presently handled except by costly numerical procedures. An example is refraction effects in variable area ducts with flow provided that the reflection effects are not dominant. Another important point is that the expression of modal properties in terms of propagation angles is nearly equivalent to an expression in terms of cut-off ratio. The same statements can thus be made in terms of propagation angles as were made in Refs. 2 to 4 in terms of cut-off ratio. Modes with nearly equivalent propagation angles will behave similarly in an acoustic liner. A group of modes with similar propagation angles can thus be treated as an entity without the need to distinguish between the individual modes. This is espe-

cially significant if a large number of propagating modes are available and carrying significant acoustic power. If a direct measurement of acoustic power in the duct can be made as a function of increments in the propagation angles, then a significant simplification will be obtained. It is possible that propagation angles may be easier to measure than cut-off ratios, although either one would be sufficient. This problem is currently being studied.

References

1. Rice, E. J., Heidmann, M. F., and Sofrin, T. G., "Modal Propagation Angles in a Cylindrical Duct with Flow and The Effect Upon Noise Radiation," AIAA Paper No. 79-0183, Jan. 1979, also NASA TM-79030, 1978.

2. Rice, E. J., "Acoustic Liner Optimum Impedance for Spinning Modes with Mode Cut-off Ratio as the Design Criterion," AIAA Paper 76-516, July 1976, also NASA TM X-73411, 1976.

3. Rice, E. J., "Inlet Noise Suppressor Design Method Based Upon the Distribution of Acoustic Power with Mode Cut-off Ratio," Advances in Engineering Science, NASA CP-2001, Vol. 3, 1976, pp. 883-894.

4. Rice, E. J., "Optimum Wall Impedance for Spinning Modes--A Correlation with Cut-off Ratio," AIAA Paper 78-193, Jan. 1978, also NASA TM-73862, 1978.

5. Wright, S. E., "Waveguides and Rotating Sources," Journal of Sound and Vibration, Vol. 25, No. 1, Nov. 8, 1972, pp. 163-178.

6. Posey, J. W., "High Frequency Sound Attenuation in Short Flow Ducts," NASA TM-78708, May 1978.

7. Tester, B. J. "The Propagation and Attenuation of Sound in Lined Ducts Containing Uniform or 'Plug' Flow," Journal of Sound and Vibration, Vol. 28, No. 2, May 22, 1973, pp. 151-203.

8. Rice, E. J., "Spinning Mode Sound Propagation in Ducts with Acoustic Treatment," NASA TN D-7913, 1975.

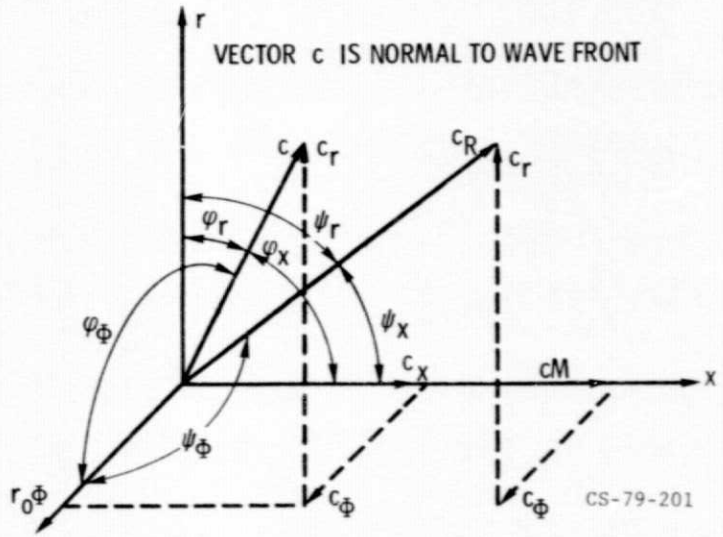

Figure 1. - Sketch of the propagation angles and vectors in the duct.

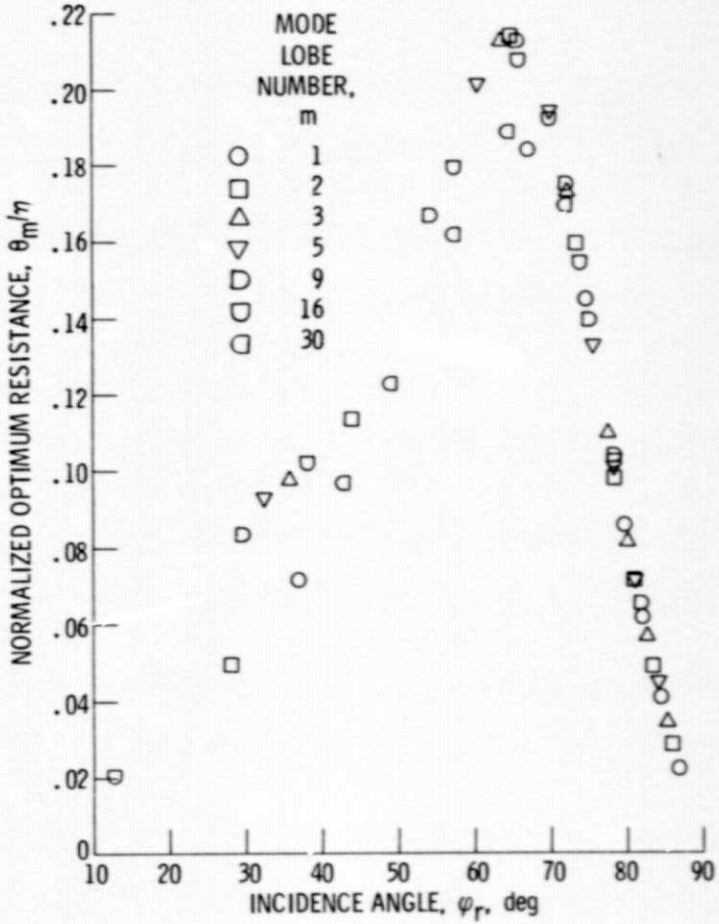

Figure 2. - Correlation of optimum resistance with wave incidence angle on the wall, $\eta = 15$, $M_0 = -0.4$, $\epsilon = 0.05$.

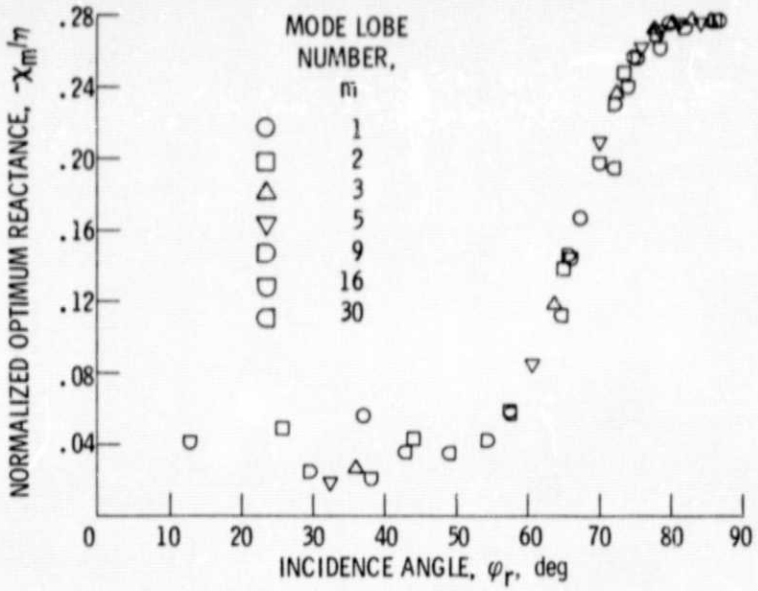

Figure 3. - Correlation of optimum reactance with wave incidence angle on the wall, $\eta = 15$, $M_0 = -0.4$, $\varepsilon = 0.05$.

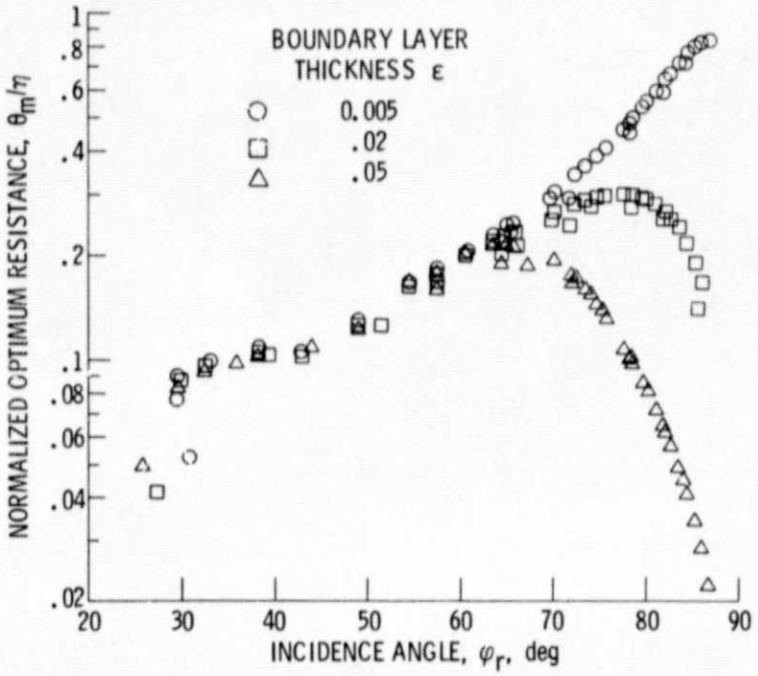

Figure 4. - Effect of boundary layer thickness upon optimum resistance-incidence angle correlation, $\eta = 15$, $M_0 = -0.04$.

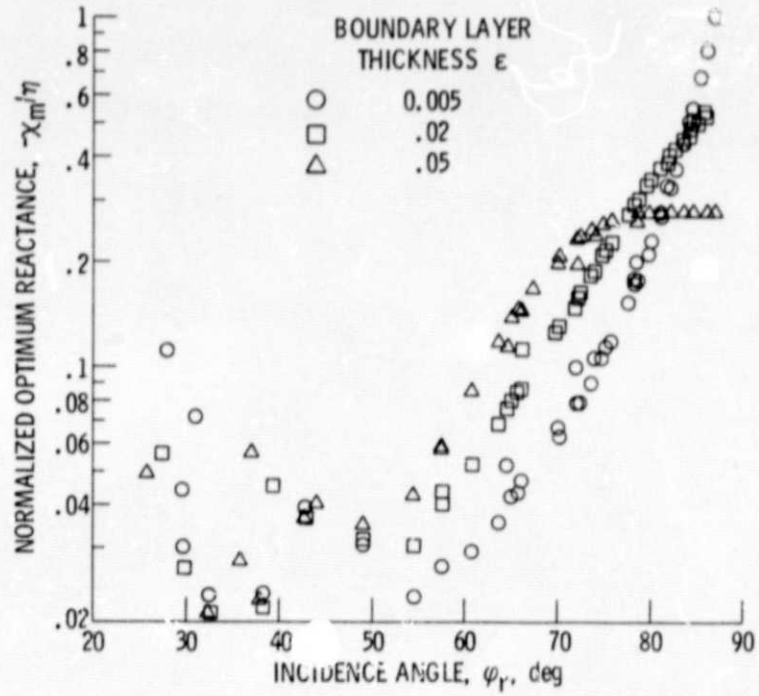

Figure 5. - Effect of boundary layer thickness upon optimum reactance-incidence angle correlation, $\eta = 15$, $M_0 = -0.4$.

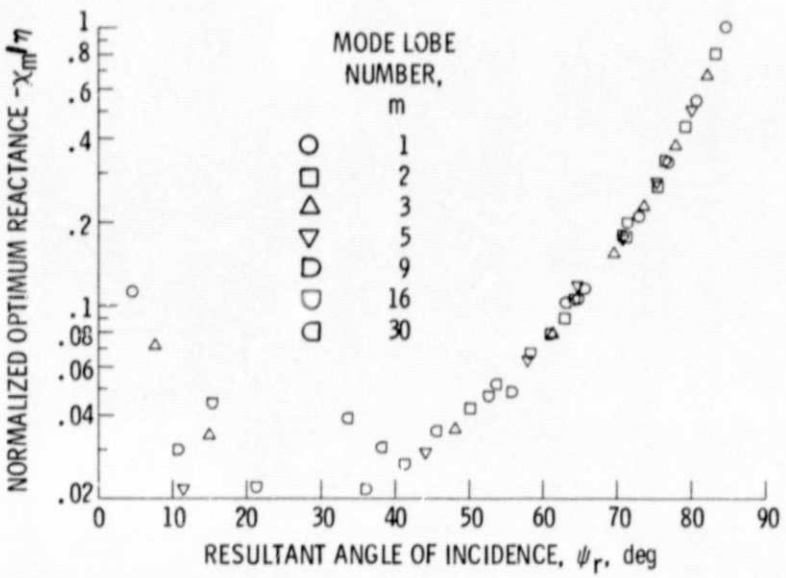

Figure 6. - Correlation of optimum reactance with resultant incidence angle, $\varepsilon = 0.005$, $\eta = 15$, $M_0 = -0.4$.

E-6202

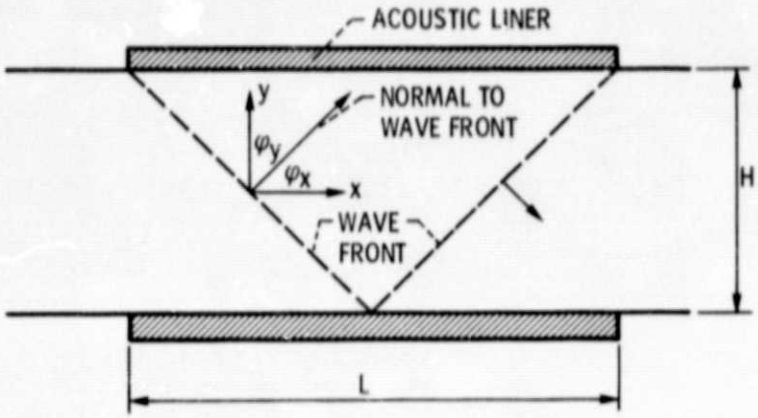

Figure 7. - Sketch of wave front and propagation angles in a rectangular duct.

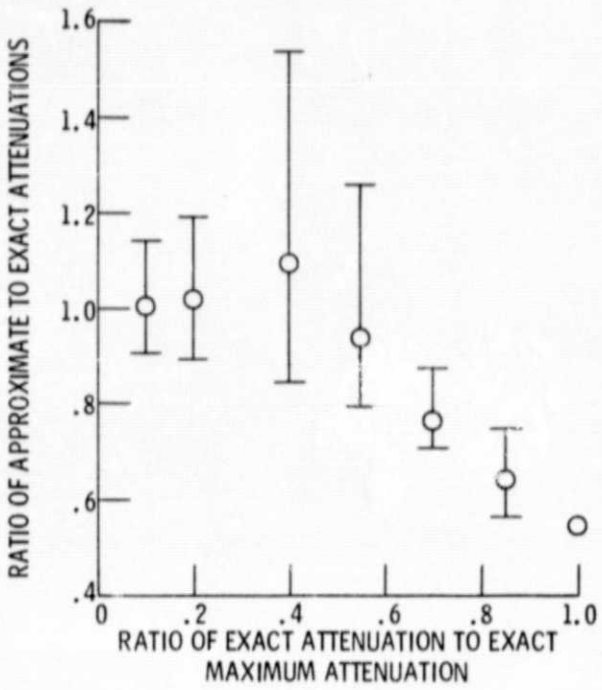

Figure 8. - Comparison of approximate and exact calculated attenuations over the complete attenuation range, rectangular duct, second symmetric mode, M = 0, η = 5.

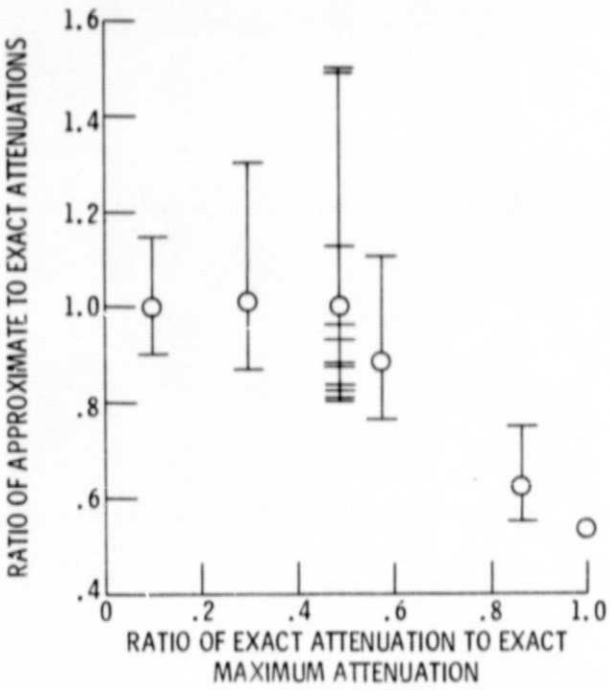

Figure 9. - Comparison of approximate and exact calculated attenuations over the complete attenuation range, rectangular duct, second symmetric mode, $M = -0.4$, $\eta = 5$.

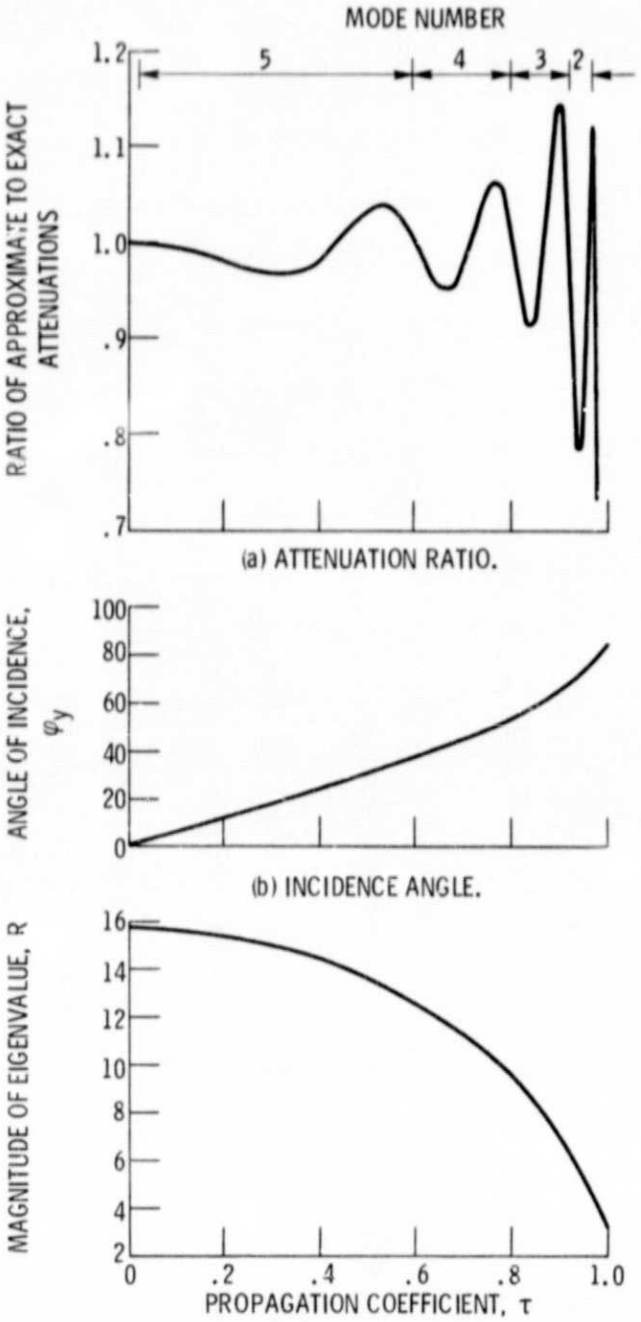

Figure 10. - Propagation calculations made over entire range of propagation coefficient, τ, rectangular duct, $M = 0$, $\sigma = 0.02$, $\eta = 5$.

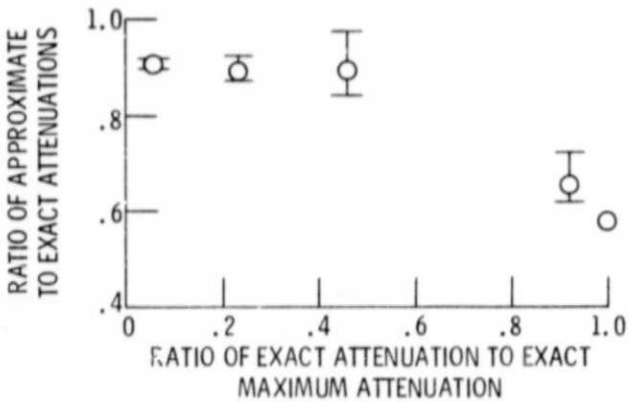

Figure 11. - Comparison of approximate and exact calculated attenuations over the complete attenuation range, cylindrical duct, seven lobed spinning mode, second radial, $M = 0$, $\eta = 20$.